Centrifugally spun hybrid polyhydroxyalkanoate/dextran nanocapsule fiber matrix for the delivery of hydrophilic payloads

Sourav Nayak (1,2)[†], Chris Vanheusden (2,3)[†], Thomas Leendertse (1,2), Lieze Schruers (1), Birte Luyck (1,2), Jorgo Merchiers (2,3), Jan D'Haen (2,4), Mieke Buntinx (2,3), Naveen Reddy (2,3) and Anitha Ethirajan (1,2)

1. Nanobiophysics and Soft Matter Interfaces group, Institute for Materials Research, Hasselt University, Wetenschapspark 1, B-3590 Diepenbeek, Belgium.

2. IMEC, associated lab IMOMEC, Wetenschapspark 1, B-3590 Diepenbeek, Belgium.

3. Materials and Packaging Research & Services, Institute for Materials Research (IMO-IMOMEC), Hasselt University, Wetenschapspark 27, 3590 Diepenbeek, Belgium

4. Analytical & Microscopical Services, Institute for Materials Research (IMO-IMOMEC), Hasselt University, Wetenschapspark 1, 3590 Diepenbeek, Belgium

[†] Both authors contributed equally.

Correspondence: anitha.ethirajan@uhasselt.be

Abstract (max. 250 words):

Biopolymeric micro- and nanofibers with active ingredients have gained significant attention for biological applications. However, the incorporation of hydrophilic compounds into hydrophobic matrices via spinning techniques remain rather unexplored. Here we report the incorporation of dextran nanocapsules (Dex-NC) in centrifugally spun poly(3-hydroxybutyrate-co-3-hydroxyhexanoate) (PHBHHx) fibers for the release of hydrophilic payloads. Inverse miniemulsion polymerization was employed to synthesize hydrophilic Dex-NCs with an average size of 0.25 µm. The Dex-NCs were embedded into PHBHHx via dual solvent centrifugal spinning at 0-7 wt.% loading, resulting in beaded fibers with average fiber diameters of 4-6 µm. The effect of Dex-NC loading on the melting and crystallization behavior of PHBHHx was limited, while the strength and stiffness of the hybrid fibers was retained. The elongation of the hybrid fiber mats is reduced with increasing Dex-NC loading, but remains suitable for biological applications. Further, the *in vitro* release measurements showed a time dependent release of embedded Dex-NCs and the payload from the hybrid fibers. We anticipate this hybrid fiber matrix to be a starting point for the development of non-woven mats for slow release of hydrophilic payloads for biological applications, especially for medical wound dressings.

Keywords: dextran, nanocapsules, poly(3-hydroxybutyrate-co-3-hydroxyhexanoate), PHBHHx, fibers, cumulative release

1. Introduction

Polymeric micro and nanofibers have gained increasing interest over decades owing to their attractive characteristics such as high aspect ratio, tunable properties, ability to form 3D networks, etc. [1-4]. Tailor made fibers with tunable composition, morphology, and structure have found applications in different fields such as tissue engineering, regenerative medicine, drug delivery, nanoparticle delivery, adsorption and filtration media, sensors, optics, textile engineering and food (packaging) systems among others [5-9]. Depending on the purpose, (non-)porous, hollow or core-shell nanofibers employing neat or blend/composite materials have been generated [10]. A wide range of synthetic polymers such as polyvinyl alcohol (PVA), polyethylene oxide (PEO), polylactic acid (PLA), polycaprolactone (PCL), and poly (lactic-co-glycolic acid) (PLGA) and natural polymers such as chitosan, dextran, cellulose, hyaluronic acid, alginate, and silk proteins have been used for generating fibers [4, 11, 12]. Depending on the polymer characteristics, as well as additives and fiber production parameters, several characteristics such as mechanical and thermal properties and porosity can be varied in the fiber material. For biomedical use, polymers that are perceived as relatively safe, biocompatible and (bio)degradable are the natural choice for fiber production.

A commonly used technique for preparing polymeric fibers (PF) is electrospinning, where an electric field is applied between the nozzle and the ground state, which overcomes the surface tension of the polymer droplet at the nozzle and thins it into a fiber [10, 13-17]. However, the electrospinning process is limited by the need of high electric fields, extra solvent extraction processes, low production outputs and long production times [18, 19]. Other techniques to fabricate fibers include phase-separation, self-assembly, melt spinning, emulsion spinning, solution blow spinning and centrifugal spinning [18]. Among these, centrifugal spinning (CFS), also known as Forcespinning™ or rotary jet spinning, overcomes many disadvantages of the widely used electrospinning [20-22]. CFS is a versatile technique as it offers high throughput, fast production rate and does not require high electric fields. In CFS, a spinning solution is fed to the rotating spinneret with two or more nozzles. Once the solution reaches the nozzle, a droplet forms and elongates into a jet due to the centrifugal forces, where after solid fibers are formed due the evaporation of the solvent [23]. The fibers can then be collected with a variety of collector systems surrounding the spinneret [24-27]. Additionally, both polymeric solutions and melt polymers can be used for the fabrication of the fibers [24, 25]. Owing to the simplicity and high production rate, several studies have been performed to make well characterized PFs using CFS, proving the latter to be a reliable and effective fiber spinning technique [21, 23, 26, 28-31].

Incorporation of (active) ingredients such as organic/inorganic fillers, nanoparticles (metal, metal oxide, polymer) allows to realize hybrid fibers with enhanced properties as they can add additional functionalities

or provide reinforcement to the structure [32]. By employing functional nanocarriers/nanocontainers within the fibers, further advanced functionalities can be realized [33]. For instance, by encapsulating active ingredients within nanocarriers, the usefulness of the former is also imparted to the fibers. Moreover, for applications such as drug delivery and tissue engineering, drugs and growth factors are needed for therapy [34-36]. By encapsulating these therapeutics, toxicity effects, premature release, and degradation of the active ingredients can be avoided [35, 37, 38]. In this regard, colloid-electrospinning, has been widely used for generating composite/hybrid fibers where electrospinning of a polymer solution was accomplished in the presence of one or several colloidal dispersions of organic and/or inorganic colloids [39-42]. Previously, nanocapsules (NCs) loaded with upconversion dyes were electrospun in a PVA matrix [43]. Crespy et al. reported embedding of redox-responsive silica nanocapsules carrying payloads into PVA nanofibers [44]. The hierarchical composite structure yielded an extra protection and enhanced control of the payload release. Mostly, aqueous dispersions were employed and various hydrophobic payloads were embedded into the fibers [40, 45]. However, for drug delivery and tissue engineering, NCs containing water soluble compounds are highly desired.

In this work, for the first time CFS is employed to embed nanocapsules containing hydrophilic compounds in polymeric fibers to yield biodegradable hybrid nanocapsule/microfibers. Such non-woven polymer fibers have gained continuous interest in the medical field. Especially, suitable medical textiles in wound care are of major concern in the health sector and have an ever-increasing demand. On average, 1-3% of total health care expenditures is needed to cover wound care expenses each year [46, 47]. Hence, medical fabric sourced from renewable resources to promote the wound healing process is intriguing, owing to the huge demand in the medical sector. In this regard, poly(3-hydroxybutyrate-co-3-hydroxyhexanoate) (PHBHHx), a medium chain length polyhydroxyalkanoate (PHA) biopolymer with semi crystalline, biobased and biodegradable characteristics, is a compelling choice to use as a fiber matrix because it is rendered less brittle and more ductile compared to other PHA family members [48, 49]. PHAs can be synthesized by bacteria from a wide range of carbon-rich substrates such as fats and sugars [50]. Recently, PHAs have been synthesized from waste-streams and second-generation feedstocks, such as waste water, animal by-products, saw dust, food waste, etc. [51-55]. Most importantly, PHAs are a competing choice among other bioplastics in terms of environmental load, versatility, and integration possibilities in current waste management systems [56]. A highly hydrophilic biopolymer dextran was chosen for the NC shell. The latter is a bacterial-derived polysaccharide consisting of glucose units linked together by α-1-6 and α-1-3 glycosidic bonds and has been widely used in biomedical applications [57, 58]. The miniemulsion technique offers a convenient route to encapsulate both hydrophobic or hydrophilic payloads in to the nanocontainers [59, 60]. To encapsulate hydrophilic payloads within the NC, inverse miniemulsion employing interfacial reaction at the droplet interface is used [61, 62].

It is worth to note that despite several advantages of the centrifugal spinning technique for generating hybrid fibers, spinning using desired solvent mixtures is still in its infancy. Previously, preparation of neomycin sulfate loaded PLA/PCL blend fibers using dichloromethane or dichloromethane/ethanol mixture (90/10) was reported [63]. The presence of ethanol as cosolvent was shown to be crucial for drug loading. However, the (co-)solvent choice is critical especially if sensitive compounds like biomolecules or growth factors will be used. As polymer solutions of PHAs for CFS also necessitate the use of low boiling solvents like chloroform or dichloromethane, the embedding of nanocapsules with preconfined hydrophilic compounds during fiber spinning is therefore highly appealing. Also, to the best of our knowledge, the proposed colloid-centrifugal spinning to embed such NCs in PHBHHx fibers using organic solvent(s) has not been explored.

Here, dextran NCs (Dex-NCs) were prepared by the inverse miniemulsion technique in cyclohexane. For hybrid fiber production, the Dex-NCs of different specific concentrations were mixed with chloroform solutions of PHBHHx with fixed concentrations. The latter was obtained by optimizing the fiber production using varying concentrations of PHBHHx in a chloroform/cyclohexane (85/15 wt.%) solvent mixture. The hybrid NC embedded PFs were obtained after colloid-centrifugal spinning using chloroform/cyclohexane solvent mixtures. The obtained hybrid fibers were characterized for their morphology, thermal and mechanical properties. Overall, we present a facile approach of embedding Dex-NCs inside the centrifugally spun PHBHHx to form hybrid fibers containing hydrophilic ingredients. Given the demand for wound care materials, non-woven fabrics made of sustainable materials that can be loaded with active therapeutic ingredients/drugs and allowing sustained release to accelerate the wound healing process are highly interesting and desired. As a proof of concept, water soluble Rhodamine B dye loaded Dex-NCs were embedded within the fibers and the payload release was characterized.

2. Materials and Methods

2.1 Materials

Toluene-2,4-diisocyanate (TDI, >98%) was purchased from Sigma Aldrich (Germany). Dextranase from *Chaetomium erraticum*, Sodium dodecyl sulfate (SDS, >99%) were obtained from sigma Aldrich (Belgium). The surfactant Hypermer™ B246 (a block copolymer containing polyhydroxystearic acid and poly(ethylene glycol)) was kindly supplied by Croda Europe Ltd (UK). Sodium chloride (NaCl, 99.8%) was obtained from Merck (Germany). The dye Rhodamine B (Rh B) (λ_{ex} = 456 nm; λ_{em} = 568 nm, >98%), cyclohexane (99.5%) were obtained from Acros Organics (Belgium). Dextran (M_n = 40000 g/mol) was purchased from ThermoFisher (Germany). Chloroform ($CHCl_3$, AnalaR NORMAPUR) and dialysis bags (MWCO 3.5 kDa) were supplied by VWR Chemicals (Belgium). PHBHHx pellets (KANEKA Biodegradable Polymer Green Planet™, M_w = 3.3 × 10^5 g/mol and PDI = 2.7) containing 10.5 mol% 3-

hydroxyhexanoate was kindly provided by Kaneka (Westerlo-Oevel, Belgium). All chemicals were used without any further purification. DI water obtained from Sartorius Stedim Biotech machine was used during all the experiments, unless mentioned. PBS buffer solution of pH 7.4 was prepared from BupH^{TM} Modified Dulbecco's Phosphate buffered saline packs (0.008 M sodium phosphate, 0.002 M potassium phosphate, 0.14 M sodium chloride, 0.0027 M potassium chloride) dissolved in 500 ml of DI water. To make the solution for pH = 5, the PBS buffer of 7.4 was adjusted with aqueous HCl solution.

2.2 Synthesis of Nanocapsules

The nanocapsules were prepared by adapting an established protocol from the group using the miniemulsion technique [61]. Briefly, a continuous phase (CP) was prepared by mixing 165 mg Hypermer B246 in 9.63 mL of cyclohexane at 65 °C, until the surfactant was completely dissolved. The dispersed phase (DP) was prepared by mixing 100 mg dextran, 20 mg NaCl salt, with or without 5 mg Rh B dye in 1.3 mL of DI water. The CP was then mixed with the DP and the mixture was stirred at 1400 rpm for 1 h at room temperature (RT) for the formation of pre-macro emulsions. Next, the mixture was ultrasonicated using a Branson 450W digital sonifier (3/16" tip) for 3 min (ON: 30 s, OFF: 20 s) with an amplitude of 70% while cooling in an ice water bath. Meanwhile, the additive phase (AP) was prepared by dissolving 35 mg Hypermer B246 in 6.42 mL cyclohexane at 65 °C. Prior to sonication, 50 µL TDI was added to the AP, and added dropwise to the ultrasonicated mixture during a period of 10 minutes. The ultrasonicated reaction mixture was then heated at 60 °C for 2 h and was further stirred overnight at RT to complete the reaction. Finally, the reaction mixture was passed through a 2 µm filter paper to remove any large aggregates.

2.3 Determination of solid content and encapsulation efficiency

The solid content (SC) of the Dex-NC dispersion in cyclohexane was determined thermogravimetrically. Briefly, 1 ml of NC solution was weighed before and after evaporating cyclohexane completely by heating at 65 °C and the SC was determined according to the following equation [64]:

$$SC\ (\%) = \frac{m_{NC}}{m_D} \times 100 \quad (1)$$

with m_{NC} = mass of dried nanocapsules and m_D = mass of 1 mL nanocapsules dispersion in cyclohexane.

The encapsulation efficiency of Rh B into Dex-NCs was determined after transferring the NCs into the water phase. This was performed by mixing 2 g of the NC dispersion in cyclohexane into 10 g 0.3 wt.% SDS water at 1400 rpm for 2 h in a closed vial. After that, the mixture was sonicated (42 kHz) in a sonication bath for 5 minutes and was stirred overnight at the same rpm while the vial cap was opened to allow the evaporation of cyclohexane at RT. Then, 1 ml of the filtered sample was centrifuged at 20000 rpm for 1 h at 8 °C to sediment down the NCs and the absorbance of Rh B in the supernatant was measured. From the

calibration curve of Rh B (supplementary material, S1), the concentration of non-encapsulated dye was measured and the encapsulation efficiency (EE) was determined according to the equation [65]:

$$EE\ (\%) = \frac{m_{Total\ dye} - m_{Free\ dye}}{m_{Total\ dye}} \times 100 \quad (2)$$

with $m_{Total\ dye}$ the mass of Rh B in 1 ml redispersed sample (calculated) and $m_{Free\ dye}$ the mass of Rh B in the supernatant. All the measurements were carried out in triplicates and the average value is reported.

2.4 Dynamic light scattering (DLS)

The average size and size distribution/polydispersity index (PDI) of the Dex-NCs were measured at 25 °C by dynamic light scattering (DLS) using a Zetasizer Ultra from Malvern Panalytical (Malvern, UK). 100 µL of Dex-NC samples were diluted with 1.5 mL cyclohexane and were measured in triplicate to obtain the average size and PDI from light scattering intensity data.

2.5 Attenuated total reflectance Fourier transform infrared spectroscopy (ATR-FTIR)

The chemical composition of the nanocapsules was analyzed by using a Bruker Tensor 27 Fourier Transform IR spectrometer. A small amount of dried Dex-NC was directly placed on the spectrometer and the spectral region was analyzed in the range from 4000 cm^{-1} to 600 cm^{-1} (16 scans)**.**

2.6 Transmission electron microscopy (TEM)

The morphology of the Dex-NCs was studied by TEM imaging using a Tecnai Spirit TEM operating at 120 kV (FEI company, Hillsboro, Oregon, USA) with an Olympus-SIS MegaView G2 CCD camera. The diluted sample in cyclohexane phase was drop casted and dried on a TEM grid (formvar foil upon copper grids, Electron Microscopy Sciences). No additional staining was performed for imaging.

2.7 Centrifugal spinning of hybrid fibers

The spinning solutions were prepared by first dissolving PHBHHx pellets in $CHCl_3$ under stirring at 55 °C for 1h at a ratio of 10 wt.%. Next, the Dex-NC dispersion in cyclohexane was added to the PHBHHx/$CHCl_3$ solution in particular amounts (based on the SC of the Dex-NC dispersion in cyclohexane) to obtain Dex-NC/PHBHHx ratios of 1, 3, 5 and 7 wt.%. Additional cyclohexane was added to obtain a cyclohexane/chloroform ratio of 15/85 wt.%. This mixture was stirred at room temperature for 1h to further homogenize. An additional dispersion containing 3 wt.% Dex-NC/PHBHHx with Rh B dye was prepared to assess the Dex-NC distribution in the produced fibers with confocal microscopy and to perform release studies. The solutions were maintained at room temperature before spinning. A lab-built CFS setup with an arm-style spinneret was used to perform the fiber spinning experiments (Figure 1) [26, 28, 30, 66]. Two aluminum nozzles with an orifice diameter of 0.6 mm were screwed onto the spinneret. The solutions were

delivered to the center of the rotating spinneret via a syringe pump to ensure a continuous flow. The rotational speed was kept constant at a speed of 4000 rpm and the collectors were set at a distance of ± 10-12 cm from the spinneret orifice. All fibers were collected with a custom-made fork and folded into fiber mats. Centrifugal fiber spinning was performed at room temperature and under a fume hood. The CFS process of the hybrid fibers is schematically shown in Figure 1.

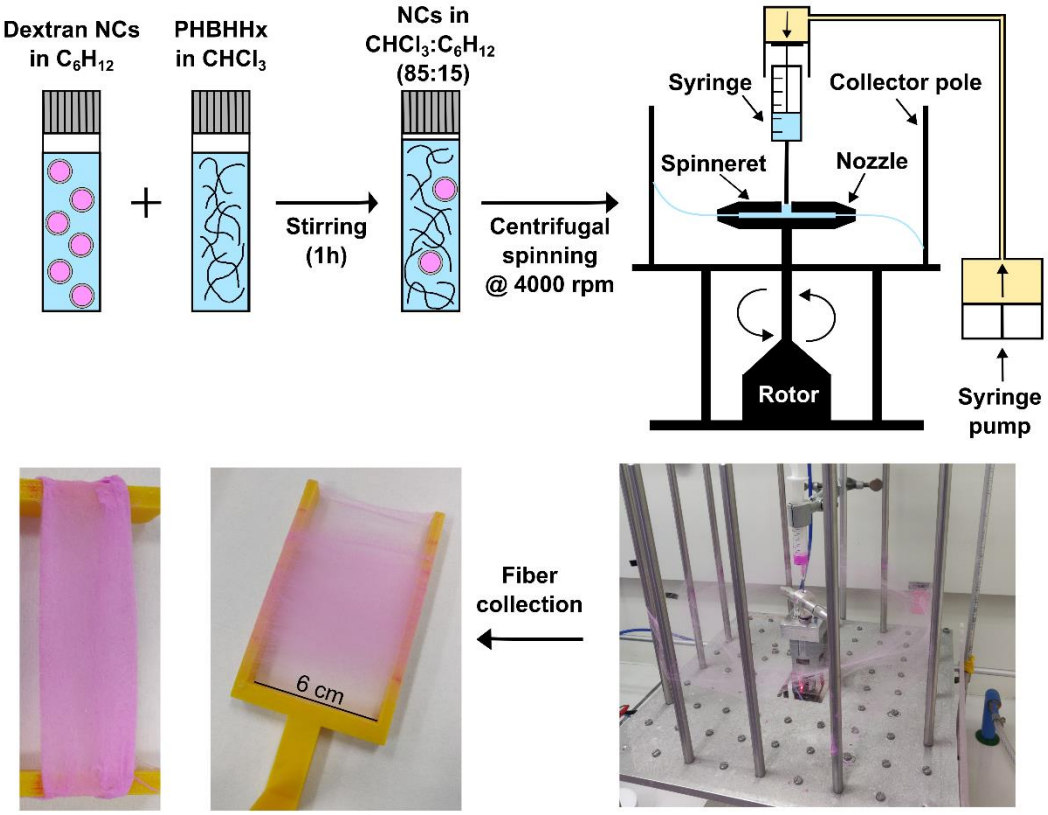

Figure 1. Schematic presentation of the CFS process of the hybrid fibers. A dispersion of dye loaded Dex-NCs in cyclohexane is stirred with a PHBHHx/chloroform solution and centrifugally spun at 4000 rpm into fibers with 0-7 wt.% Dex-NC loading. The fibers are collected with a fork and folded into fiber mats. The presented fiber mats are produced with Rh B dye loaded Dex-NCs (pink color).

2.8 Scanning electron microscopy (SEM)

The morphology of the hybrid fibers was analyzed via SEM images acquired using a Zeiss 450 FEGSEM with Gemini 2 optics (Zeiss, Oberkochen, Germany) at 10 kV under vacuum. The fibers were sputtered with a thin layer of gold-palladium before analysis to reduce charging. The distribution in fiber diameters was measured from SEM images using ImageJ software (Maryland, United States). For each sample type, the fiber diameter was measured at 100 randomly chosen fiber locations.

2.9 Optical microscopy

Morphological analysis of the hybrid fiber samples was performed using the Nikon Eclipse ME600 (Amsterdam, The Netherlands) in combination with a Nikon DS-Fi2 camera, controlled by NIS elements D software.

2.10 Confocal fluorescence microscopy

The distribution of the Rh B dye loaded Dex-NCs within the hybrid fibers was analyzed via confocal fluorescence imaging. Images were collected using a Zeiss LSM880 NLO scan head mounted on an Axio observer frame and a plan-apochromat 63x/1.4 oil DIC M27 objective. The Rh B loaded Dex-NCs were excited with a Helium-Neon laser at 543 nm. For the detection of the fibers, second harmonic generation (SHG) imaging was performed using a femtosecond pulsed laser (MaiTai DeepSee, spectra-physics) tuned at a central wavelength of 810 nm as excitation source. Emission was detected with a band-pass filter of 552-632 nm. The distribution of the Dex-NCs throughout the fibers was observed via z-stacks over the depth of the fibers. Images were taken every 0.5 µm with a pixel dwell time of 1.55 µs and a pixel size of 0.10 µm. The resulting 1352 x 1352 images were manually aligned. No further processing was performed.

2.11 Mechanical characterization

The mechanical properties of the hybrid fibers were studied by tensile testing using a benchtop 5ST universal tester (Tinius Olsen, Redhill, UK). The tensile testing set-up is shown in Figure 2. Folded fiber mat samples with a width of 1-2 cm were cut to a length of 6 cm and were pasted in between paper frames for better handling and to avoid slippage at the clamp grips. The paper frame was cut prior to tensile testing. The fiber mats were loaded between two clamps at a distance of 20 mm and were tested with a preload of 0.1 N, a pre-load speed of 1 mm/min and a crosshead speed of 10 mm/min. The fiber mat cross-sectional area (A) was calculated with the weight of the sample (m), the mat length (L) and the polymer density (ρ = 1.19 g/cm^3), $A = m/\rho L$. The tensile strength (σ) was calculated as the peak stress, and the Young's modulus (E) was calculated from the linear slope at low strains (3-5 %). The elongation at break was determined as the strain (%) at about 95% peak load drop. The fiber mats were conditioned for at least 3 days at 23 °C and 50% relative humidity (RH) before tensile testing. The mechanical properties are reported as the average of 5 measurements.

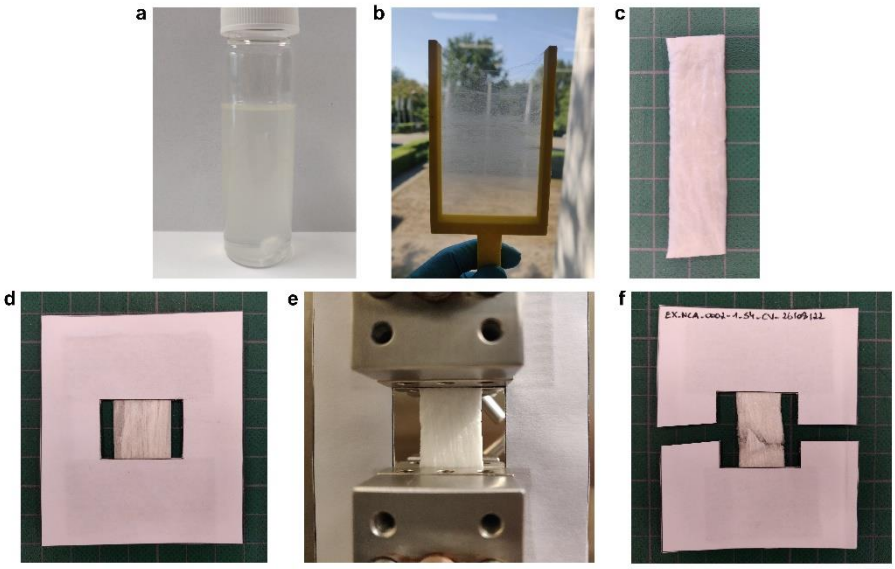

Figure 2. Centrifugally spun hybrid fiber samples. (a) Mixed PHBHHx/$CHCl_3$ spinning solution (b) collected spun fibers, (c) prepared fiber mat, (d) framed sample before tensile testing, (e) sample during tensile testing and (f) sample after tensile testing.

2.12 Thermal characterization

Differential scanning calorimetry (DSC) (Q200 instrument, TA Instruments, USA) was used to evaluate the melting and crystallization properties of the hybrid fibers. Fiber mat samples of about 4-6 mg (0, 1, 3, 5 and 7 wt.% Dex-NCs loaded in PHBHHx) were sealed in aluminum pans and heated from -30 °C to 160 °C before being kept isothermal for 2 min. The samples were cooled to -30 °C and kept isothermal for 2 min before heating to 160 °C. The measurements were performed under nitrogen atmosphere (50 ml/min N_2) and the heating/cooling rates were set at 20 °C/min. The degree of crystallinity (X_c) of the samples was calculated with the following equation:

$$X_c = \frac{\Delta H_m}{\Delta H_m^0 \times \omega_{PHBHHx}} \times 100 \quad (3)$$

with ΔH_m the melting enthalpy from the first heating scan, ΔH_m^0 the melting enthalpy of the 100% crystalline sample (115 J/g [67, 68]) and ω_{PHBHHx} the weight fraction of PHBHHx in the nanocomposites. The crystallization enthalpy ΔH_c was derived from the first cooling scan. The thermal properties are reported as the average of 3 measurements.

2.13 Cumulative release study

Cumulative release experiments were carried out following the reported procedure in literature [69, 70]. As the dye is encapsulated within the Dex-NCs, the release of the Dex-NCs from the fiber mat as well as the dye release from the Dex-NCs were assessed. The Dex-NC release experiment was carried out by incubating

a piece of ~ 1 × 1 cm^2 (33 mg) of 3 wt.% Dex-NC (containing Rh B dye) loaded PHBHHx fiber mat into 10 ml of buffer solutions (PBS) with pH levels of 7.4 and 5.0 respectively, while stirring at 100 rpm at 37 °C. At different time intervals, 2 ml of the release medium was taken out and was replaced with fresh 2 ml buffer solution. The absorbance ($A_{Rh\ B}$) of the collected solutions was measured at 554 nm and the concentration of the released NCs was calculated using a standard calibration curve of Rh B in buffers (supplementary material, S1 and S2). The cumulative release of Dex-NCs (%) was calculated according to the following equation:

$$\text{Cumulative release} = \frac{V_e \sum_1^{n-1} C_i + V_o C_n}{M_o} \times 100 \quad (4)$$

with V_e the volume of release media removed every time (2 ml), V_o the total volume of release media (10 ml), C_n and C_i are the concentration of Rh B in the release media and M_o is the total mass of Rh B entrapped in the fiber mat.

The second release experiment included the use of Dextranase enzyme solution to check the Dex-NC degradability. A piece of ~ 1 × 1 cm^2 (33 mg) of 3 wt.% fiber mats (with Rh B) was transferred into a dialysis bag containing 2 ml of dextranase with a concentration of 2 mg/ml. The dialysis bag (MWCO 3.5 kDa) was then immersed into 8 ml of buffer solution (pH = 7.4), maintaining a total of 10 ml release medium while stirring at 100 rpm at 37 °C. The rest of the protocol is similar to the previous one.

2.14 Swelling experiments

The swelling of the hybrid fibers was measured by immersing ~ 5 mg of 0, 1, 3 and 7 wt.% of fibers into glass vials containing 5 ml of buffer solutions (PBS), respectively. The degree of swelling was tested in two different buffer solutions of pH 7.4 and 5.0 under stirring at room temperature for 24 hours. The weight of the fiber mats was measured before and after the incubation. The excess water from the swelled fibers was absorbed by clean wipes [71, 72]. The degree of swelling (DS) is calculated with the following equation:

$$DS = \frac{W_S - W_D}{W_D} \quad (5)$$

with W_S the weight of the fibers after swelling and W_D the weight of fibers before swelling. The measurements were performed in duplicate and average values were represented.

2.15 Contact angle measurements

Water contact angle experiments (Sessile drops) were performed with a DataPhysics instrument (Filderstadt, Germany) and SCA 20 software. Water droplets of 5 µl were deposited on the surface of 0, 1, 3 and 7 wt.% hybrid fibers using a Hamilton syringe. The contact angle at time zero was obtained by extrapolating the

linear part of the contact angle versus time curve by linear regression. The contact angle is reported as the average of 5 measurements.

3. Results and Discussion

3.1 Synthesis and characterization of dextran nanocapsules

Miniemulsion interfacial polymerization is a versatile technique for the preparation of nanocarrier dispersions [73, 74]. High shear force (ultrasound) is usually applied to an emulsion of water in oil or oil in water. Due to the high shear force, small nanometer sized droplets are formed that are stabilized by the presence of surfactants [75]. In this study, inverse miniemulsion was applied, where the water droplets containing dextran, Rh B dye and a hydrophilic salt (NaCl) were stabilized by the polymeric surfactant Hypermer B246 in cyclohexane. The interfacial crosslinking reaction was performed by heating the reaction mixture at 60 °C using the crosslinker TDI in the organic phase. Three different batches of Dex-NCs were prepared separately and mixed together to obtain a large volume of NC solution for mixing with the PHBHHx/$CHCl_3$ solutions for fiber fabrication. The average hydrodynamic diameter (D_h) of the NCs in the final solution was found to be ~ 0.25 µm with PDI of ~ 0.17 (supplementary material, Figure S3.1). The average solid content of the solution was around 1.52 wt.%. To increase the solid content of the solution, the cyclohexane phase was evaporated by heating until half of the volume was achieved, which resulted in a solid content of around 3 wt.%. The average encapsulation efficiency of the NC dispersion in water was 86 ± 3.7%.

The NC morphology was confirmed by TEM imaging which showed a core shell morphology of the nanocapsules (Figure 3). Solid black crystals inside the NCs correspond to the salt crystals as reported previously [62]. As the NCs have soft shells, the NCs tend to collapse and also aggregate. This might be attributed to the sample preparation, where the sample solution is placed on the TEM grid and air dried.

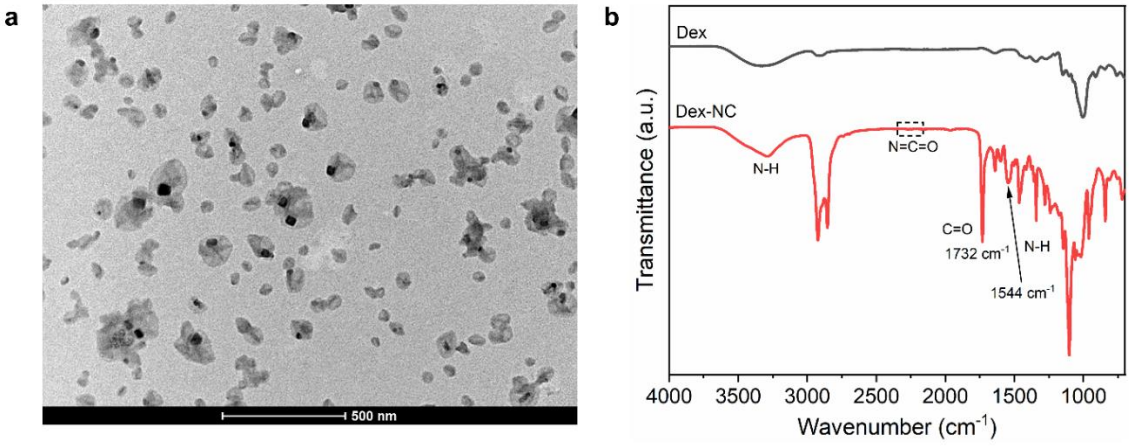

Figure 3. (a) Representative TEM image of Rh B loaded Dex-NCs used for generating hybrid fiber matrix via colloid-CFS and (b) FTIR spectra of the pure dextran and crosslinked Dex-NCs.

The interfacial crosslinking between -OH/-NCO was expected (supplementary material, Scheme S3.2) and was confirmed by FTIR spectroscopy measurements. A typical spectrum of pure dextran and dried dextran NCs are presented in Figure 3b. Pure dextran shows broad -OH stretching vibration beyond 3026 cm^{-1} and other peaks from the monomeric glucose units. In the Dex-NCs spectrum, -NH stretching peak is observed at 3286 cm^{-1} and NH bending at 1544 cm^{-1} in accordance with the literature [65, 76]. The carbonyl vibration at 1732 cm^{-1} and the N-H vibration at 1544 cm^{-1} are strong evidence for the formation of urethane groups. The vibration at 1638 cm^{-1} (the carbonyl of urea groups) indicates that the side reaction of isocyanate with water occurred, leading to urea units. The flat signal at 2276 cm^{-1} indicates complete consumption of -NCO groups of TDI [77].

3.2 Production and characterization of hybrid fiber/NC

3.2.1 Hybrid fiber morphology and Dex-NC embedment

Since the Dex-NCs were synthesized in a cyclohexane phase, the hybrid fibers were produced from a dual solvent system containing chloroform and cyclohexane. Chloroform ensures sufficient dissolution of the PHBHHx polymer, while cyclohexane is necessary for the transfer of the NCs to the spinning solution. The suitable ratio of chloroform/cyclohexane in the spinning solution was experimentally determined to be 85/15 wt.% in order for PHBHHx to be fully dissolved without precipitation. In this way, the fiber morphology is mainly determined by a combination of both the spinning parameters and the dual solvent system. The morphology of the hybrid fibers can influence the thermal, mechanical and/or release properties of the fabricated mats. Therefore, the morphology and diameters of hybrid fibers with different Dex-NC loadings (0, 1, 3, 5 and 7 wt.%) were analyzed from SEM images as shown in Figure 4. Optical microscopy images of the fibers can be consulted in Figure S4. The fiber diameter slightly increases upon addition of NCs, with an average diameter of $\overline{D}_f$ = 4.2 ± 1.0 µm at 0 wt.% NCs to $\overline{D}_f$ = 5.8 ± 1.5 µm at 7 wt.% NCs. However, no significant difference in fiber diameter distribution is apparent for different NC loadings. The fiber diameter distributions with corresponding average ($\overline{D}_f$) and median ($\widetilde{D}_f$) fiber diameters are shown in Figure S5. In comparison, we previously reported the fabrication of centrifugally spun PHBHHx fibers with a similar polymer concentration (10-12 wt.%) using chloroform as the only solvent and showed that the fiber diameter can be reduced from the micrometer range to the nanometer range at lower polymer concentrations [78].

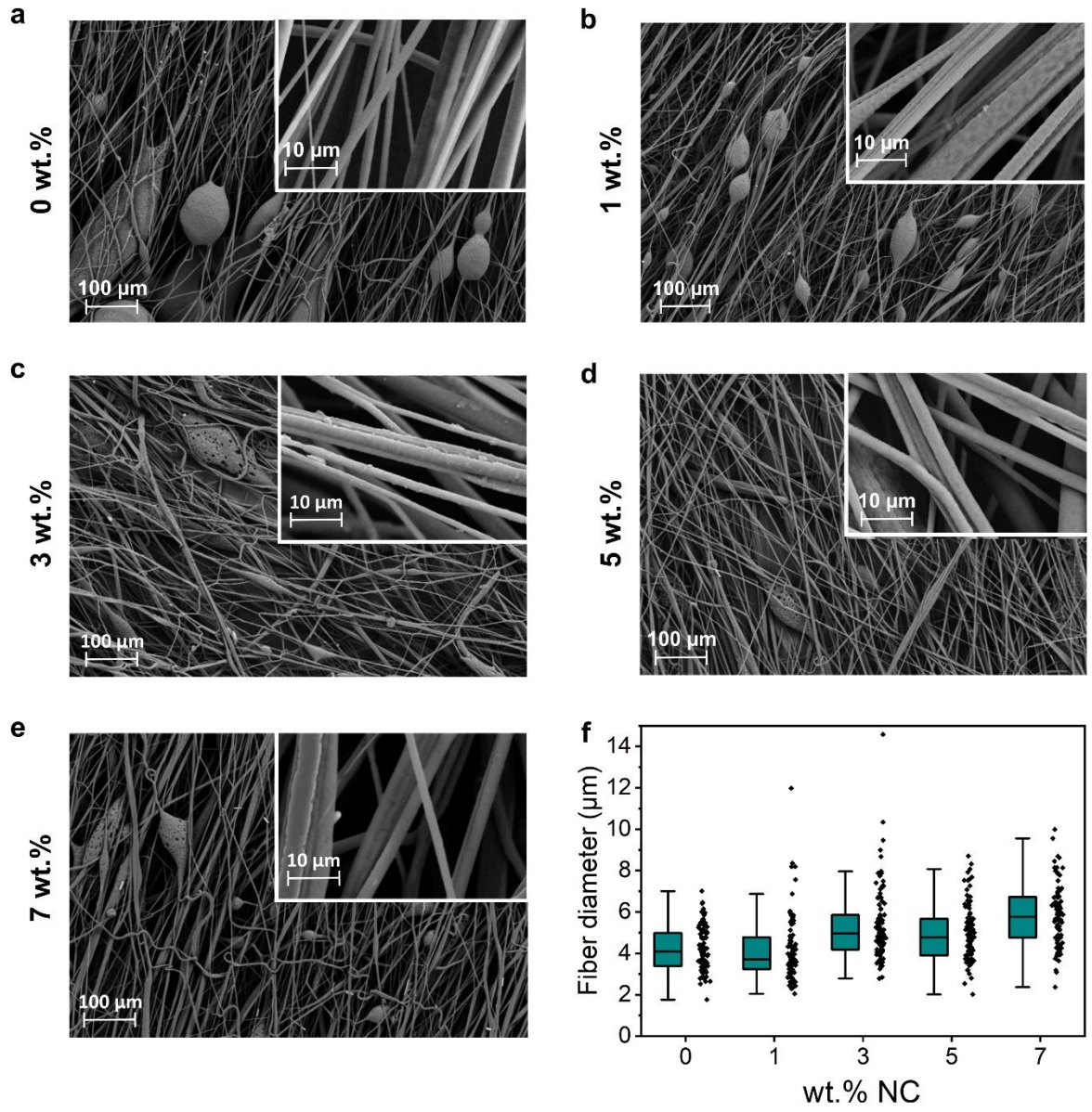

Figure 4. SEM images of hybrid fibers with 0-7 wt.% Dex-NCs (a-e) and the diameter of hybrid fibers spun with different Dex-NC concentrations (f). The box is determined by the 25th and 75th percentiles, and the horizontal solid lines and whiskers show the median fiber diameter and the range within 1.5 of the IQR (interquartile range), respectively.

The hybrid fibers show beaded or beads-on-a-string (BOAS) morphology for all Dex-NC loadings and no clear change in morphology is detected with increasing Dex-NC loading. Some small sized particles or clustered particles were also observed on the fiber surface, which could be attributed to the presence of Dex-NCs agglomerates. The formation of beads could be explained by a lack of sufficient visco-elastic forces. Golecki et al. showed that increasing solvent volatility can decrease fiber beading [79]. Therefore, the addition of less volatile solvents such as cyclohexane to the chloroform rich spinning solution can explain

the obtained beaded fibers. The fibers do clearly exhibit bead formation, while the majority of beads show irregular pore formation. It is believed that a phase separation of a polymer-rich (chloroform) and a polymer-poor (cyclohexane) phase occurs. The highly volatile chloroform is quickly evaporating during CFS, increasing the relative content of the cyclohexane (with lower volatility) to form a two-phase heterogeneous binary solution [80]. After solidification of the jet during spinning, the polymer-poor phase and condensed water droplets on the jet surface leave imprints that form pores [81]. The pores collapse on the surface of the fibers due to extensive elongation of the jet, while the pores in the beads are retained due to insufficient stretching, explaining the formation of irregular pores in the beads [81].

Previous research on fiber spinning mainly focused on the improvement of beaded and BOAS fibers into continuous fibers. However, the unique features of BOAS fibrous structures recently gained more interest for use, especially in drug delivery applications to reduce the burst release and to maintain a more sustained release of the drug [82]. The alleviation of the burst release can be explained by the proper encapsulation of the drugs in the beads and by increasing the distance for diffusion from the polymer to the medium [82, 83]. In addition, burst release can be reduced with increasing bead size [84, 85]. For these reasons, the centrifugally spun fibers with targeted beads and BOAS morphology with a dual solvent system can be advantageous.

The distribution of the Dex-NCs in the PHBHHx fiber matrix was visualized via confocal laser scanning microscopy. An overview of three different cross-sections of hybrid fibers obtained via the z-stack technique is shown in Figure 5. Brightfield images were taken to visualize the fiber matrix. Second harmonic generation (SHG) was utilized to image the fibers, while the NCs were loaded with the hydrophilic dye Rh B (λ_{ex} = 456 nm; λ_{em} = 568 nm) for fluorescence imaging. The confocal images demonstrate the embedment of the Dex-NCs in the fiber matrix. The nanocarriers are randomly distributed throughout the whole fiber length, where the brighter spots are likely due to aggregation of NCs. Since the confocal images confirm the random embedment of the NCs in the PHBHHx fiber matrix, it is assumed that the NCs are also present in the beads.

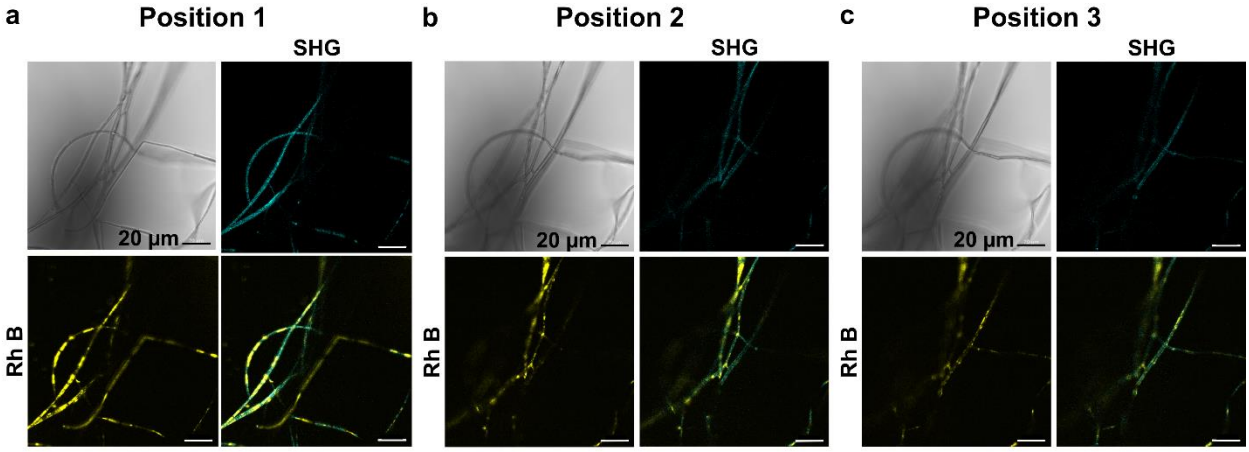

Figure 5. Confocal microscopy images of the hybrid fibers (3 wt.% Dex-NCs) for multiple focal planes (z-stack, a-c).

3.2.2 Hybrid fiber thermal properties

The influence of Dex-NCs on the melting and crystallization behavior of PHBHHx in the hybrid fibers was investigated with DSC. The heating and cooling scans of the hybrid fibers with different NC loading are shown in Figure 6. The characteristic values are summarized in Table 1. The first heating scan shows the melting behavior of the as-spun hybrid fibers which is mainly defined by the multiple melting behavior of PHBHHx [86]. The first endothermic peak at $T_{m,1}$ originates from the melting of primary crystals formed during initial crystallization, while the second endothermic peak at $T_{m,2}$ is due to the melting of crystals formed by reorganization or thickening during DSC heating [86, 87]. The two endothermic peaks $T_{m,1}$ and $T_{m,2}$ arise at temperatures of ~112-115 °C and ~126 °C, respectively. The variation in $T_{m,1}$ is independent of the NC loading, indicating a limited effect of the NCs on the melting behavior of PHBHHx. The crystallinity of the polymeric fibers (calculated based on the weight fraction of PHBHHx) decreases slightly with increasing NC loading, from 36.5% at 0 wt.% NCs to 33.1% at 7 wt.% NCs. This indicates that the dextran NCs can influence the packing of PHBHHx polymer chains to a small extent during crystallization from the solution during CFS. A minor endothermic transition around 50 °C is also present in the first heating scan, arising from some crystals formed during storage at room temperature [87].

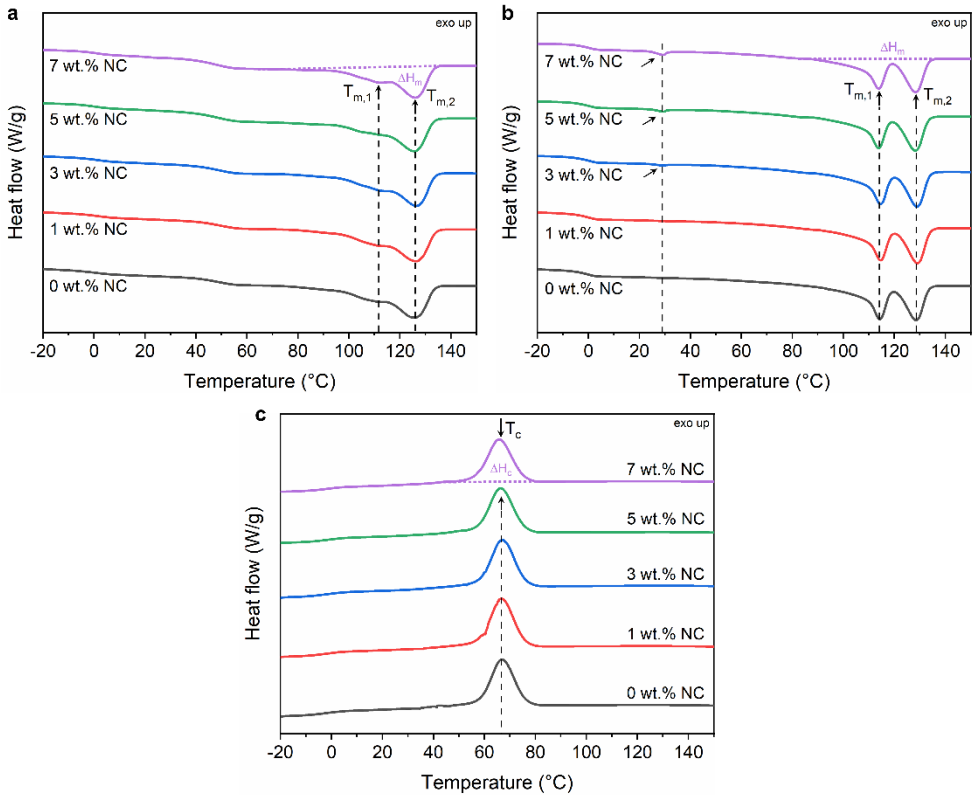

Figure 6. DSC thermograms of the (a) first heating, (b) second heating and (c) first cooling cycles of the hybrid fibers loaded with 0, 1, 3, 5 and 7 wt.% Dex-NCs.

The second heating cycle represents the thermal history of the material after controlled cooling during DSC and exhibits two endothermic melting peaks $T_{m,1}$ and $T_{m,2}$ at ~113-114 °C and ~128-129 °C, respectively. The melting peaks are slightly shifted to lower temperatures at NCs loadings of 5 and 7 wt.%. However, the melting enthalpy remains similar upon NC loading, around ~36 J/g, indicating no significant influence of the NCs on the melting behavior of PHBHHx. The glass transition temperature occurs around 0 °C, as previously reported in literature [88]. In addition, an endothermic event arises around 30 °C for 3-7 wt.% NCs and is more pronounced at higher NC loading. This endothermic transition is attributed to the melting process associated with the components of Dex-NCs itself, which comprises of dispersed phase ingredients, including crosslinked dextran, and Hypermer polymeric surfactant as confirmed by DSC scans shown in Figure S6 (supplementary information). Additionally, the event is not due to endothermal effects of dextran itself, as also shown in the DSC scan (Figure S6). The first cooling scan shows a crystallization peak temperature ($T_{c,p}$) at 66-67 °C and a crystallization enthalpy of 33-34 J/g for all NC loadings, suggesting that the NCs do not negatively influence the crystallization of the PHBHHx polymer.

Table 1. Thermal properties of the centrifugally spun hybrid fibers with different Dex-NC loading (0-7 wt.%) for DSC 1st heating, 1st cooling and 2nd heating cycles (20°C/min heating/cooling rate) (n=3, ± 1 SD).

PHBHHx/ NC*	1st heating			2nd heating		
	$T_{m,1}$ (°C)	$T_{m,2}$ (°C)	X_c (%)	$T_{m,1}$ (°C)	$T_{m,2}$ (°C)	ΔH_m (J/g)
0 wt.%	113.2 ± 0.6	125.8 ± 0.2	36.5 ± 1.0	114.6 ± 0.2	128.8 ± 0.2	35.7 ± 0.2
1 wt.%	113.5 ± 0.2	126.2 ± 0.2	35.3 ± 0.1	114.6 ± 0.0	129.1 ± 0.2	35.8 ± 0.2
3 wt.%	115.2 ± 0.5	126.4 ± 0.1	34.5 ± 0.8	114.7 ± 0.1	129.0 ± 0.1	36.2 ± 0.5
5 wt.%	113.0 ± 1.4	125.8 ± 0.2	33.8 ± 0.7	113.8 ± 0.1	128.3 ± 0.0	37.0 ± 0.3
7 wt.%	112.4 ± 0.3	126.0 ± 0.2	33.1 ± 1.6	113.8 ± 0.1	128.2 ± 0.2	36.1 ± 0.5

PHBHHx/ NC*	1st cooling	
	$T_{c,p}$ (°C)	ΔH_c (J/g)
0 wt.%	66.9 ± 0.1	33.1 ± 0.9
1 wt.%	67.1 ± 0.3	33.5 ± 0.9
3 wt.%	67.0 ± 0.1	34.2 ± 0.3
5 wt.%	66.4 ± 0.1	33.5 ± 0.7
7 wt.%	65.9 ± 0.2	33.2 ± 0.6

*Melting peaks are denoted as $T_{m,1}$ and $T_{m,2}$, crystallinity content as X_c, crystallization peak temperature as $T_{c,p}$, and melting and crystallization enthalpies as ΔH_m and ΔH_c respectively. The enthalpy values are calculated and presented according to the polymer weight fraction in the hybrid fibers.

In summary, the DSC results indicate that the melting and crystallization behavior of PHBHHx in the hybrid fibers is not clearly altered upon loading of dextran NCs and only a slight reduction in crystallinity is apparent. We conclude that the loading of dextran NCs up to concentrations of 7 wt.% seems feasible to maintain the thermal properties of PHBHHx.

3.2.3 Hybrid fiber/NC mechanical properties

The tensile properties of the produced fiber mats can give an indication of their strength and stretchability, which is important for use in applications like wound dressings. In addition, no severe reduction of the fiber mat strength and elasticity upon loading of the NCs should be apparent. Therefore, the mechanical properties of the hybrid fiber mats were investigated with tensile testing and the obtained results and representative stress-strain curves are shown in Figure 7. The average tensile strength (σ) shows an increasing trend upon addition of NCs, from 2.7 ± 0.5 MPa at 0 wt.% NCs to a maximum of 3.5 ± 0.5 MPa at 5 wt.% NCs. A similar effect is apparent for the Young's modulus (E), from 30 ± 15 MPa at 0 wt.% NCs to a maximum of 42 ± 10 MPa at 5 wt.% NCs. In contrast, a decreasing trend of the average elongation at break upon addition of NCs is apparent, from 141 ± 5 % at 0 wt.% NCs to 88 ± 8 % at 7 wt.% NCs. These results indicate that the strength and stiffness of the PHBHHx fiber mats is maintained upon loading of Dex-NCs up to 7 wt.%. The reduced elongation at break of the fibers at higher Dex-NC loading can be explained by the fact that agglomerated Dex-NCs can act as stress concentrators. Despite the reduced elongation at break of the fiber

mats with increased NC loading, the stretchability remains in the same order of magnitude and seems appropriate for use in biomedical applications such as wound dressing [89]. A decrease in elongation at break for beaded PLGA fibers with 5 wt.% of BSA-dextran particle loading was also reported previously [85]. However, this decrease in ductility was accompanied with a reduction in tensile strength and Young's modulus, in contrast to our results.

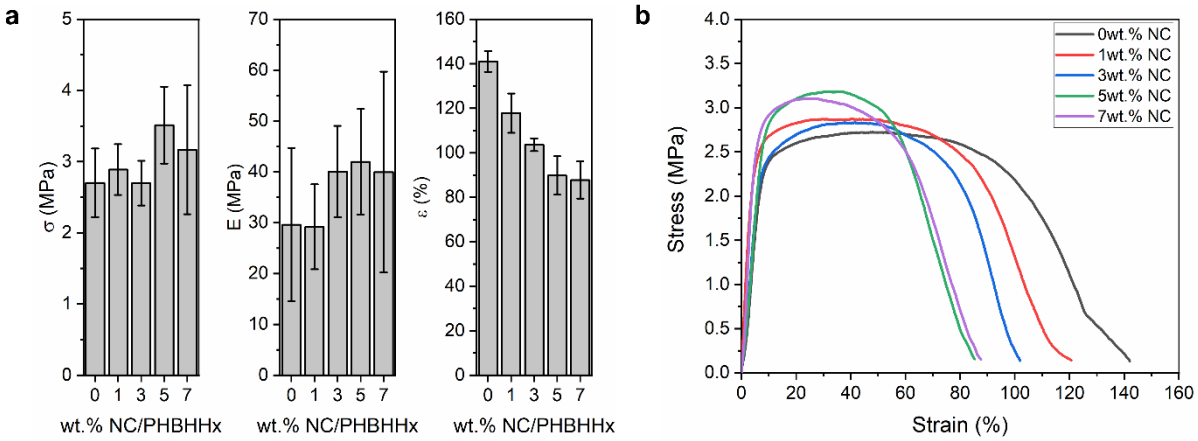

Figure 7. (a) The mechanical properties tensile strength (σ), Young's modulus (E), and elongation at break (ε) (n = 5), (error bars represent SD), and (b) representative stress-strain curves for hybrid fibers loaded with 0, 1, 3, 5 and 7 wt.% Dex-NCs.

3.2.4 Surface wettability and swelling of the hybrid fiber/ NC

The swelling experiments of the fibers were performed using 0, 1, 3 and 7 wt.% of Dex-NC loaded fibers to understand the release of NCs from the fibers and the results are shown in Figure 8. It was observed that with increase of NC loading in the fibers, the swelling degree increased, suggesting the retained water in the fibers. This increment could be attributed to the swelling of the dextran capsules, water uptake at the porous beads and fibers [90], and also possibly physical disintegration of the fiber mats with time. The pH effect on swelling was prominent in all the cases. All the fibers showed increased swelling at pH = 7.4 rather than in pH = 5. A similar type of swelling was observed in electrospun PVA-Dextran NFs [71].

The surface wettability of the hybrid fibers was investigated with water contact angle measurements to further understand the impact on dye release. The contact angles for PHBHHx fibers and hybrid fibers with different Dex-NC content show no clear differences and exhibit hydrophobic characteristics (CA = 132-135°), as shown in Figure 8. The contact angle of the fiber mats is mainly determined by the hydrophobic nature of the polymer and surface structure of the fiber mats, combining roughness effects of both fibers and beads. Exemplary images of the contact angle measurements are shown in Figure S7 (supplementary materials).

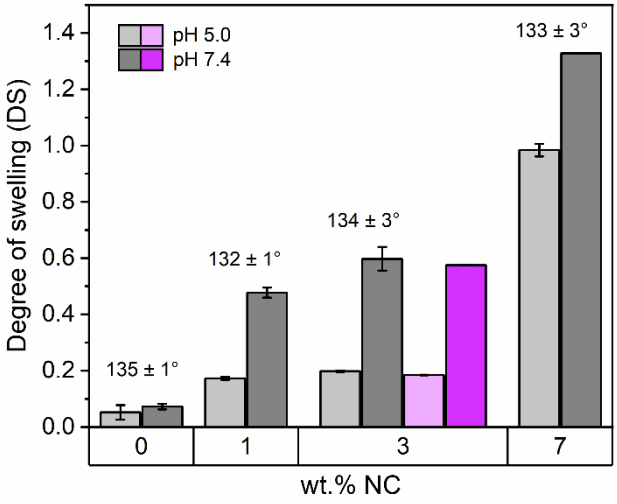

Figure 8. Degree of swelling of hybrid fiber mats (0, 1, 3 and 7 wt.% Dex-NC) in aqueous buffer (PBS) solutions with pH of 5.0 and 7.4 (n = 2, ± 1 SD) and water contact angles (n = 5, ± 1 SD) for hybrid fiber mats (0, 1, 3 and 7 wt.% Dex-NC) showing hydrophobic nature. The light and dark grey bars indicate a pH of 5.0 and 7.4, respectively. The purple bars indicate samples with Rh B loaded Dex-NCs.

3.3 Release studies of the hybrid fiber/NC

In vitro release measurements were performed to check the release of the hydrophilic dye from the hydrophobic PHBHHx polymer matrix. As the dye is encapsulated within the Dex-NCs, the release of the Dex-NCs from the fiber mat due to the disintegration of the fiber mat as well as the dye release from the Dex-NCs can be followed up by measuring the absorbance of the dye in the solution. It could be anticipated that the presence of Rh B in the release media could be due to the release of dye loaded Dex-NCs as well as the free Rh B released from the hybrid mat embedded Dex-NCs. Therefore, the release kinetics of dye loaded Dex-NC from the fiber mat and release of free Rh B from the hybrid fibers were studied independently. For the latter, the release of the dye from the Dex-NCs in the presence of a dextran degrading enzyme was carried out. The release of the Dex-NC and the free dye were followed up by evaluating the optical characteristics of the solutions under different conditions (supplementary material, Table S8.1). Firstly, Rh B incorporated 3 wt.% Dex-NC loaded PHBHHx fiber mats were incubated into the buffer solutions (PBS) of pH 5.0 and 7.4 respectively and the results are shown in Figure 9a. Approximately 22% of the dye intensity was found in the release media within 143 hours of incubation at pH 5.0 while a slightly higher release of ~25% was observed at pH 7.4, respectively. Under these conditions, the measured dye signal can be expected from the Rh B incorporated Dex-NCs released from the fiber mats (fiber surface and porous beads) due to the fiber mat disintegration. The degradation of the hydrophobic PHBHHx via hydrolysis over time could also contribute to the release of Dex-NCs. However, no clear reduction of the fiber molecular weight was evidenced for 0 wt% Dex-NC/PHBHHx fibers after 24 h of swelling, as measured by DSC (Figure S8.6 and Table S8.7) and GPC (Table S8.8).

At the beginning of the experiments, the fiber mat was found to be floating on the buffer solution and a non-wettability behavior was observed. With time, the fiber mats started to swell and sink in the release media suggesting favorable fiber and solution interaction to release the NCs (Figure 9a inset). The presence of NCs in the release media was analyzed further by DLS and the measurement indicated the presence of colloidal features (Figure S8.2). However, the findings were inconclusive likely due to the low concentration of NCs. Therefore, to confirm the release of Dex-NCs in the release media, a 7 wt% Dex-NCs loaded fiber mat was incubated with PBS buffer (pH = 7.4) and the analytes in the release media was verified by independent techniques, namely FTIR and DLS (Figure S8.3 and Figure S8.4). The presence of dextran hydroxy(-OH) peaks in the FTIR spectra of release media confirmed the release of Dex-NCs from the fiber mats, as well as the NCs were better measurable with DLS. Additionally, the thermal properties of the fibers were also studied. However, no clear change in thermal properties was apparent for 7 wt% Dex-NCs loaded fibers before and after the release for 5 days (Figure S8.9).

To validate the release of the cargo dye Rh B from the fibers, another fiber mat was incubated into a dialysis bag containing dextranase enzyme solution to facilitate dextran hydrolysis from the NCs and to release the dye. The latter was used to ensure that the measured signal in the media is arising from the free dye and not from the dye associated with the intact Dex-NCs (as it cannot pass through the dialyzing membrane bag). Figure 9b indicates the release graph in presence of dextranase, showing ~23% of Rh B release within 94 hours of incubation (supplementary material, Table S8.4). Interestingly, the dye release was faster with dextranase while no particle population was found by DLS of the release media. The image in the inset (Figure 9b) visually shows the presence of the dye in the medium outside of the dialysis bag. From the release experiments, a time dependent release of the hydrophilic dye from the hybrid fiber/NC could be confirmed.

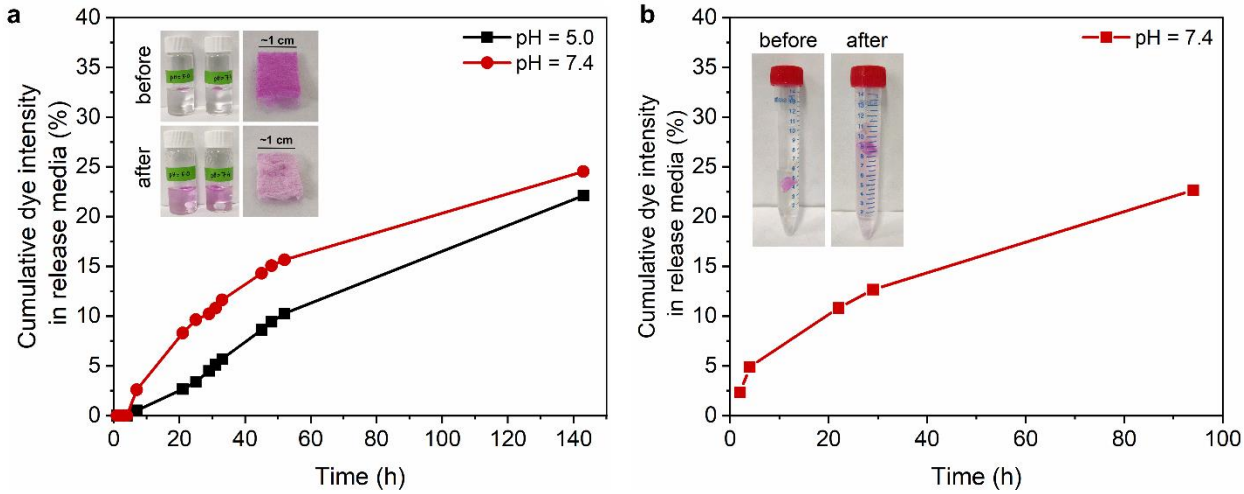

Figure 9. Cumulative release of Rh B loaded NCs from the hybrid fibers measured using UV-Vis spectroscopy at pH levels of 5.0 and 7.4 (a) and in the presence of dextranase at a pH level of 7.4 (b). The images show a visual decrease of dye coloration from the fiber mat before and after release (a) and an increase of dye color in the buffer solution (PBS) after release in presence of dextranase (b).

4. Conclusions

This study shows the successful embedding of hydrophilic Dex-NCs into a hydrophobic PHBHHx fiber matrix by centrifugal spinning using a dual solvent system. The Dex-NCs allow for facile encapsulation of hydrophilic payloads. Bead formation in the hybrid fibers was found to be irrespective of the NC loading and no clear difference was observed in fiber diameter with increase in NC loading. The effect of NC loading did not clearly alter the melting and crystallization behavior of the PHBHHx fibers. The tensile strength and Young's modulus of the hybrid fiber mats were retained, but the elongation behavior of the hybrid NCs was reduced as expected with the increase of NC loading. Further, cumulative release experiments revealed a time dependent release of the NCs from the fiber matrix. Overall, the study shows the potential of Dex-NC loaded PHBHHx fibers with sufficient mechanical properties in biological applications for the delivery of hydrophilic payloads. In the future, in vitro cell studies are planned to assess the biological applicability using suitable payloads and additional functionalities to the Dex-NCs by incorporating responsive moieties that can be exogenously triggered.

5. **CRediT authorship contribution statement**

Sourav Nayak: Conceptualization, Methodology, Investigation, Writing - Original Draft, Formal analysis, Visualization. **Chris Vanheusden**: Conceptualization, Methodology, Investigation, Writing - Original Draft, Formal analysis, Visualization. **Thomas Leendertse**: Validation, Investigation, Writing - Original Draft, Formal analysis, Visualization. **Lieze Schruers**: Investigation, Writing - Review & Editing. **Birte Luyck**: Investigation, Writing - Original Draft. **Jorgo Merchiers**; Investigation, Writing - Review & Editing. **Jan D'Haen**: Resources, Visualization, Writing - Review & Editing. **Mieke Buntinx**:. Writing - Review & Editing, Supervision, Project administration, Funding acquisition. **Naveen Reddy**: Conceptualization, Writing - Review & Editing, Supervision, Funding acquisition. **Anitha Ethirajan**: Conceptualization, Methodology, Writing - Review & Editing, Formal analysis, Supervision, Project administration, Funding acquisition.

6. Declaration of Competing Interest

The authors declare no conflict of interest.

7. Acknowledgements

The authors acknowledge Prof. Roos Peeters (Materials and Packaging Research & Services, IMO-IMOMEC, UHasselt) for access to the tensile tester and Prof. Wouter Marchal (Analytical & Circular

Chemistry, IMO-IMOMEC, UHasselt) for providing access to the DSC equipment. Bart Ruttens and Hilde Pellaers (Analytical & Microscopical Services, IMO-IMOMEC, UHasselt) are thanked for kindly measuring the SEM samples. The Advanced Optical Microscopy Centre at Hasselt University is acknowledged for support with the microscopy experiments. Microscopy was made possible by the Research Foundation Flanders (FWO, project G0H3716N). This research was partially funded by the Special Research Fund (BOF) of Hasselt University, grant number BOF20DOC06.

8. References

1. Medeiros ES, Glenn GM, Klamczynski AP, Orts WJ, Mattoso LHC. Solution blow spinning: A new method to produce micro- and nanofibers from polymer solutions. J Appl Polym Sci. 2009;113(4):2322-30. DOI: 10.1002/app.30275
2. Long Y-Z, Li M-M, Gu C, Wan M, Duvail J-L, Liu Z, et al. Recent advances in synthesis, physical properties and applications of conducting polymer nanotubes and nanofibers. Prog Polym Sci. 2011;36(10):1415-42. DOI: 10.1016/j.progpolymsci.2011.04.001
3. Tan EPS, Lim CT. Mechanical characterization of nanofibers – A review. Compos Sci Technol. 2006;66(9):1102-11. DOI: 10.1016/j.compscitech.2005.10.003
4. Ding J, Zhang J, Li J, Li D, Xiao C, Xiao H, et al. Electrospun polymer biomaterials. Prog Polym Sci. 2019;90:1-34. DOI: 10.1016/j.progpolymsci.2019.01.002
5. Huang Z-M, Zhang YZ, Kotaki M, Ramakrishna S. A review on polymer nanofibers by electrospinning and their applications in nanocomposites. Compos Sci Technol. 2003;63(15):2223-53. DOI: 10.1016/S0266-3538(03)00178-7
6. dos Santos DM, Correa DS, Medeiros ES, Oliveira JE, Mattoso LHC. Advances in Functional Polymer Nanofibers: From Spinning Fabrication Techniques to Recent Biomedical Applications. ACS Appl Mater Interfaces. 2020;12(41):45673-701. DOI: 10.1021/acsami.0c12410
7. Ghafoor B, Aleem A, Najabat Ali M, Mir M. Review of the fabrication techniques and applications of polymeric electrospun nanofibers for drug delivery systems. J Drug Delivery Sci Technol. 2018;48:82-7. DOI: 10.1016/j.jddst.2018.09.005
8. Torres-Giner S. 5 - Electrospun nanofibers for food packaging applications. In: Lagarón J-M, editor. Multifunctional and Nanoreinforced Polymers for Food Packaging: Woodhead Publishing; 2011. p. 108-25. DOI: 10.1533/9780857092786.1.108
9. Huang H, Song Y, Zhang Y, Li Y, Li J, Lu X, et al. Electrospun Nanofibers: Current Progress and Applications in Food Systems. J Agric Food Chem. 2022;70(5):1391-409. DOI: 10.1021/acs.jafc.1c05352
10. Wang C, Wang J, Zeng L, Qiao Z, Liu X, Liu H, et al. Fabrication of electrospun polymer nanofibers with diverse morphologies. Molecules. 2019;24(5):834. DOI: 10.3390/molecules24050834
11. Rogina A. Applied Surface Science Electrospinning process: Versatile preparation method for biodegradable and natural polymers and biocomposite systems applied in tissue engineering and drug delivery. Appl Surf Sci. 2014;296:221-30. DOI: 10.1016/j.apsusc.2014.01.098
12. Lee K, Nam H, editors. Jeong. SDD: High Performance Code Clone Detection System for Large Scale Source Code Companion to the 20th Annual ACM SIGPLAN Conference on Object-Oriented Programming, Systems, Languages, and Applications (OOPSLA'05); 2005. DOI: 10.1145/1094855.1094903
13. Xue J, Xie J, Liu W, Xia Y. Electrospun nanofibers: new concepts, materials, and applications. Acc Chem Res. 2017;50(8):1976-87. DOI: 10.1021/acs.accounts.7b00218
14. Xue J, Wu T, Dai Y, Xia Y. Electrospinning and electrospun nanofibers: Methods, materials, and applications. Chemical reviews. 2019;119(8):5298-415. DOI: 10.1021/acs.chemrev.8b00593
15. Ibrahim HM, Klingner A. A review on electrospun polymeric nanofibers: Production parameters and potential applications. Polym Test. 2020;90:106647. DOI: 10.1016/j.polymertesting.2020.106647

16. Sarkar K, Gomez C, Zambrano S, Ramirez M, de Hoyos E, Vasquez H, et al. Electrospinning to Forcespinning™. Mater Today. 2010;13(11):12-4. DOI: 10.1016/S1369-7021(10)70199-1
17. Oliveira JE, Mattoso LHC, Orts WJ, Medeiros ES. Structural and Morphological Characterization of Micro and Nanofibers Produced by Electrospinning and Solution Blow Spinning: A Comparative Study. Adv Mater Sci Eng. 2013;2013:409572. DOI: 10.1155/2013/409572
18. Lou L, Osemwegie O, Ramkumar SS. Functional nanofibers and their applications. Ind Eng Chem Res. 2020;59(13):5439-55. DOI: 10.1021/acs.iecr.9b07066
19. Patlan R, Mejias J, McEachin Z, Salinas A, Lozano K. Fabrication and Characterization of Poly(L-lactic Acid) Fiber Mats Using Centrifugal Spinning. Fibers Polym. 2018;19(6):1271-7. DOI: 10.1007/s12221-018-7063-0
20. Rogalski JJ, Bastiaansen CWM, Peijs T. Rotary jet spinning review – a potential high yield future for polymer nanofibers. Nanocomposites. 2017;3(4):97-121. DOI: 10.1080/20550324.2017.1393919
21. Zhang X, Lu Y. Centrifugal spinning: an alternative approach to fabricate nanofibers at high speed and low cost. Polym Rev 54: 677–701. 2014. DOI: 10.1080/15583724.2014.935858
22. He J, Zhou Y. Multineedle electrospinning. Electrospinning: Nanofabrication and Applications: Elsevier; 2019. p. 201-18. DOI: 10.1016/B978-0-323-51270-1.00006-6
23. Atıcı B, Ünlü CH, Yanilmaz M. A review on centrifugally spun fibers and their applications. Polymer Reviews. 2022;62(1):1-64. DOI: 10.1080/15583724.2021.1901115
24. Padilla-Gainza V, Morales G, Rodríguez-Tobías H, Lozano K. Forcespinning technique for the production of poly(d,l-lactic acid) submicrometer fibers: Process–morphology–properties relationship. J Appl Polym Sci. 2019;136(22):47643. DOI: 10.1002/app.47643
25. Stojanovska E, Canbay E, Pampal ES, Calisir MD, Agma O, Polat Y, et al. A review on non-electro nanofibre spinning techniques. RSC Adv. 2016;6(87):83783-801. DOI: 10.1039/C6RA16986D
26. Merchiers J, Meurs W, Deferme W, Peeters R, Buntinx M, Reddy NK. Influence of Polymer Concentration and Nozzle Material on Centrifugal Fiber Spinning. Polymers. 2020;12(3):575. DOI: 10.3390/polym12030575
27. Mellado P, McIlwee HA, Badrossamay MR, Goss JA, Mahadevan L, Parker KK. A simple model for nanofiber formation by rotary jet-spinning. Appl Phys Lett. 2011;99(20):203107. DOI: 10.1063/1.3662015
28. Merchiers J, Slykas CL, Martínez Narváez CD, Buntinx M, Deferme W, Peeters R, et al. Fiber Engineering Trifecta of Spinnability, Morphology, and Properties: Centrifugally Spun versus Electrospun Fibers. ACS Appl Polym Mater. 2022;4(3):2022-35. DOI: 10.1021/acsapm.1c01865
29. Merchiers J, Martínez Narváez CDV, Slykas C, Buntinx M, Deferme W, D'Haen J, et al. Centrifugally spun poly(ethylene oxide) fibers rival the properties of electrospun fibers. J Polym Sci. 2021;59(22):2754-62. DOI: 10.1002/pol.20210424
30. Merchiers J, Martínez Narváez CD, Slykas C, Reddy NK, Sharma V. Evaporation and rheology chart the processability map for centrifugal force spinning. Macromolecules. 2021;54(23):11061-73. DOI: 10.1021/acs.macromol.1c01799
31. Ding B, Wang X, Yu J. Electrospinning: nanofabrication and applications: William Andrew; 2018. DOI: 0128134410
32. Pyrgiotakis G, McDevitt J, Bordini A, Diaz E, Molina R, Watson C, et al. A chemical free, nanotechnology-based method for airborne bacterial inactivation using engineered water nanostructures. Environ Sci: Nano. 2014;1(1):15-26. DOI: 10.1039/C3EN00007A
33. Jiang S, Lv L-P, Landfester K, Crespy D. Nanocontainers in and onto Nanofibers. Acc Chem Res. 2016;49(5):816-23. DOI: 10.1021/acs.accounts.5b00524
34. Patra JK, Das G, Fraceto LF, Campos EVR, Rodriguez-Torres MdP, Acosta-Torres LS, et al. Nano based drug delivery systems: recent developments and future prospects. J Nanobiotechnol. 2018;16(1):71. DOI: 10.1186/s12951-018-0392-8
35. Mitchell MJ, Billingsley MM, Haley RM, Wechsler ME, Peppas NA, Langer R. Engineering precision nanoparticles for drug delivery. Nat Rev Drug Discovery. 2021;20(2):101-24. DOI: 10.1038/s41573-020-0090-8

36. Wilczewska AZ, Niemirowicz K, Markiewicz KH, Car H. Nanoparticles as drug delivery systems. Pharmacol Rep. 2012;64(5):1020-37. DOI: 10.1016/S1734-1140(12)70901-5
37. Deng S, Gigliobianco MR, Censi R, Di Martino P. Polymeric Nanocapsules as Nanotechnological Alternative for Drug Delivery System: Current Status, Challenges and Opportunities. Nanomaterials. 2020;10(5):847. DOI: 10.3390/nano10050847
38. De Jong WH, Borm PJ. Drug delivery and nanoparticles: applications and hazards. Int J Nanomed. 2008;3(2):133-49. DOI: 10.2147/ijn.s596
39. Wessel C, Ostermann R, Dersch R, Smarsly BM. Formation of Inorganic Nanofibers from Preformed TiO2 Nanoparticles via Electrospinning. J Phys Chem C. 2011;115(2):362-72. DOI: 10.1021/jp108202b
40. Friedemann K, Turshatov A, Landfester K, Crespy D. Characterization via Two-Color STED Microscopy of Nanostructured Materials Synthesized by Colloid Electrospinning. Langmuir. 2011;27(11):7132-9. DOI: 10.1021/la104817r
41. Li M, Zhang J, Zhang H, Liu Y, Wang C, Xu X, et al. Electrospinning: A Facile Method to Disperse Fluorescent Quantum Dots in Nanofibers without Förster Resonance Energy Transfer. Adv Funct Mater. 2007;17(17):3650-6. DOI: 10.1002/adfm.200700241
42. Friedemann K, Corrales T, Kappl M, Landfester K, Crespy D. Facile and Large-Scale Fabrication of Anisometric Particles from Fibers Synthesized by Colloid-Electrospinning. Small. 2012;8(1):144-53. DOI: 10.1002/smll.201101247
43. Wohnhaas C, Friedemann K, Busko D, Landfester K, Baluschev S, Crespy D, et al. All Organic Nanofibers As Ultralight Versatile Support for Triplet–Triplet Annihilation Upconversion. ACS Macro Lett. 2013;2(5):446-50. DOI: 10.1021/mz400100j
44. Jiang S, Lv L, Li Q, Wang J, Landfester K, Crespy D. Tailoring nanoarchitectonics to control the release profile of payloads. Nanoscale. 2016;8(22):11511-7. DOI: 10.1039/C6NR00917D
45. Stoiljkovic A, Ishaque M, Justus U, Hamel L, Klimov E, Heckmann W, et al. Preparation of water-stable submicron fibers from aqueous latex dispersion of water-insoluble polymers by electrospinning. Polymer. 2007;48(14):3974-81. DOI: 10.1016/j.polymer.2007.04.050
46. Olsson M, Järbrink K, Divakar U, Bajpai R, Upton Z, Schmidtchen A, et al. The humanistic and economic burden of chronic wounds: A systematic review. Wound Repair Regener. 2019;27(1):114-25. DOI: 10.1111/wrr.12683
47. Human Wounds and Its Burden: An Updated Compendium of Estimates. Advances in Wound Care. 2019;8(2):39-48. DOI: 10.1089/wound.2019.0946
48. Atiwesh G, Mikhael A, Parrish CC, Banoub J, Le T-AT. Environmental impact of bioplastic use: A review. Heliyon. 2021;7(9):e07918. DOI: 10.1016/j.heliyon.2021.e07918
49. Ragaert P, Buntinx M, Maes C, Vanheusden C, Peeters R, Wang S, et al. Polyhydroxyalkanoates for Food Packaging Applications. Reference Module in Food Science: Elsevier; 2019. DOI: 10.1016/b978-0-08-100596-5.22502-x
50. Anjum A, Zuber M, Zia KM, Noreen A, Anjum MN, Tabasum S. Microbial production of polyhydroxyalkanoates (PHAs) and its copolymers: A review of recent advancements. Int J Biol Macromol. 2016;89:161-74. DOI: 10.1016/j.ijbiomac.2016.04.069
51. Gutschmann B, Huang B, Santolin L, Thiele I, Neubauer P, Riedel SL. Native feedstock options for the polyhydroxyalkanoate industry in Europe: A review. Microbiol Res. 2022;264:127177. DOI: 10.1016/j.micres.2022.127177
52. Brigham CJ, Riedel SL. The Potential of Polyhydroxyalkanoate Production from Food Wastes. Appl Food Biotechnol. 2019;6(1):7-18. DOI: 10.22037/afb.v6i1.22542
53. Yukesh Kannah R, Dinesh Kumar M, Kavitha S, Rajesh Banu J, Kumar Tyagi V, Rajaguru P, et al. Production and recovery of polyhydroxyalkanoates (PHA) from waste streams – A review. Bioresour Technol. 2022;366:128203. DOI: 10.1016/j.biortech.2022.128203
54. Ganesh Saratale R, Cho S-K, Dattatraya Saratale G, Kadam AA, Ghodake GS, Kumar M, et al. A comprehensive overview and recent advances on polyhydroxyalkanoates (PHA) production using various organic waste streams. Bioresour Technol. 2021;325:124685. DOI: 10.1016/j.biortech.2021.124685

55. Kucera D, Benesova P, Ladicky P, Pekar M, Sedlacek P, Obruca S. Production of Polyhydroxyalkanoates Using Hydrolyzates of Spruce Sawdust: Comparison of Hydrolyzates Detoxification by Application of Overliming, Active Carbon, and Lignite. Bioengineering. 2017;4(2):53. DOI: 10.3390/bioengineering4020053
56. Nandakumar A, Chuah J-A, Sudesh K. Bioplastics: A boon or bane? Renewable Sustainable Energy Rev. 2021;147:111237. DOI: 10.1016/j.rser.2021.111237
57. Hu Q, Lu Y, Luo Y. Recent advances in dextran-based drug delivery systems: From fabrication strategies to applications. Carbohydr Polym. 2021;264:117999. DOI: 10.1016/j.carbpol.2021.117999
58. Sun G, Mao JJ. Engineering dextran-based scaffolds for drug delivery and tissue repair. Nanomedicine. 2012;7(11):1771-84. DOI: 10.2217/nnm.12.149
59. Weiss CK, Landfester K. Miniemulsion Polymerization as a Means to Encapsulate Organic and Inorganic Materials. In: van Herk AM, Landfester K, editors. Hybrid Latex Particles: Preparation with (Mini)emulsion Polymerization. Berlin, Heidelberg: Springer Berlin Heidelberg; 2010. p. 185-236. DOI: 10.1007/12_2010_61
60. Ethirajan A, Landfester K. Functional Hybrid Materials with Polymer Nanoparticles as Templates. Chemistry – A European Journal. 2010;16(31):9398-412. DOI: 10.1002/chem.201001477
61. Seneca S, Pramanik SK, D'Olieslaeger L, Reekmans G, Vanderzande D, Adriaensens P, et al. Nanocapsules with stimuli-responsive moieties for controlled release employing light and enzymatic triggers. Mater Chem Front. 2020;4(7):2103-12. DOI: 10.1039/D0QM00244E
62. Kuypers S, Pramanik SK, D'Olieslaeger L, Reekmans G, Peters M, D'Haen J, et al. Interfacial thiol–isocyanate reactions for functional nanocarriers: a facile route towards tunable morphologies and hydrophilic payload encapsulation. Chemical Communications. 2015;51(87):15858-61. DOI: 10.1039/C5CC05258K
63. Hongthipwaree T, Sriamornsak P, Seadan M, Suttiruengwong S. Effect of cosolvent on properties of non-woven porous neomycin-loaded poly(lactic acid)/polycaprolactone fibers. Materials Today Sustainability. 2020;10:100051. DOI: 10.1016/j.mtsust.2020.100051
64. Peters M, Desta D, Seneca S, Reekmans G, Adriaensens P, Noben J-P, et al. PEGylating poly(p-phenylene vinylene)-based bioimaging nanoprobes. Journal of Colloid and Interface Science. 2021;581:566-75. DOI: 10.1016/j.jcis.2020.07.145
65. Thongchaivetcharat K, Jenjob R, Seidi F, Crespy D. Programming pH-responsive release of two payloads from dextran-based nanocapsules. Carbohydr Polym. 2019;217:217-23. DOI: 10.1016/j.carbpol.2019.04.023
66. Merchiers J, Reddy NK, Sharma V. Extensibility-Enriched Spinnability and Enhanced Sorption and Strength of Centrifugally Spun Polystyrene Fiber Mats. Macromolecules. 2022;55(3):942-55. DOI: 10.1021/acs.macromol.1c02164
67. Xie Y, Noda I, Akpalu YA. Influence of cooling rate on the thermal behavior and solid-state morphologies of polyhydroxyalkanoates. J Appl Polym Sci. 2008;109(4):2259-68. DOI: 10.1002/app.28278
68. Vandewijngaarden J, Murariu M, Dubois P, Carleer R, Yperman J, Adriaensens P, et al. Gas Permeability Properties of Poly (3-hydroxybutyrate-co-3-hydroxyhexanoate). J Polym Environ. 2014;22:501-7. DOI: 10.1007/s10924-014-0688-1
69. Deng H, Zhao X, Liu J, Zhang J, Deng L, Liu J, et al. Synergistic dual-pH responsive copolymer micelles for pH-dependent drug release. Nanoscale. 2016;8(3):1437-50. DOI: 10.1039/C5NR06745F
70. Li B, Shan M, Di X, Gong C, Zhang L, Wang Y, et al. A dual pH- and reduction-responsive anticancer drug delivery system based on PEG–SS–poly(amino acid) block copolymer. RSC Adv. 2017;7(48):30242-9. DOI: 10.1039/C7RA04254J
71. Kenawy E-RS, Kamoun EA, Eldin MS, Soliman HMA, El-Moslamy SH, El-Fakharany EM, et al. Electrospun PVA–Dextran Nanofibrous Scaffolds for Acceleration of Topical Wound Healing: Nanofiber Optimization, Characterization and In Vitro Assessment. Arabian J Sci Eng. 2023;48(1):205-22. DOI: 10.1007/s13369-022-06856-9

72. Kamoun EA, Chen X, Mohy Eldin MS, Kenawy E-RS. Crosslinked poly(vinyl alcohol) hydrogels for wound dressing applications: A review of remarkably blended polymers. Arabian J Chem. 2015;8(1):1-14. DOI: 10.1016/j.arabjc.2014.07.005
73. Landfester K. Miniemulsion Polymerization and the Structure of Polymer and Hybrid Nanoparticles. Angew Chem, Int Ed. 2009;48(25):4488-507. DOI: 10.1002/anie.200900723
74. Tiarks F, Landfester K, Antonietti M. Preparation of Polymeric Nanocapsules by Miniemulsion Polymerization. Langmuir. 2001;17(3):908-18. DOI: 10.1021/la001276n
75. Delmas T, Piraux H, Couffin A-C, Texier I, Vinet F, Poulin P, et al. How To Prepare and Stabilize Very Small Nanoemulsions. Langmuir. 2011;27(5):1683-92. DOI: 10.1021/la104221q
76. Jagielski N, Sharma S, Hombach V, Mailänder V, Rasche V, Landfester K. Nanocapsules Synthesized by Miniemulsion Technique for Application as New Contrast Agent Materials. Macromolecular Chemistry and Physics. 2007;208(19-20):2229-41. DOI: 10.1002/macp.200700254
77. Alkanawati MS, da Costa Marques R, Mailänder V, Landfester K, Thérien-Aubin H. Polysaccharide-Based pH-Responsive Nanocapsules Prepared with Bio-Orthogonal Chemistry and Their Use as Responsive Delivery Systems. Biomacromolecules. 2020;21(7):2764-71. DOI: 10.1021/acs.biomac.0c00492
78. Vanheusden C, Vanminsel J, Reddy N, Samyn P, D'Haen J, Peeters R, et al. Fabrication of poly(3-hydroxybutyrate-co-3-hydroxyhexanoate) Fibers Using Centrifugal Fiber Spinning: Structure, Properties and Application Potential. Polymers. 2023;15(5):1181. DOI: 10.3390/polym15051181
79. Golecki HM, Yuan H, Glavin C, Potter B, Badrossamay MR, Goss JA, et al. Effect of Solvent Evaporation on Fiber Morphology in Rotary Jet Spinning. Langmuir. 2014;30(44):13369-74. DOI: 10.1021/la5023104
80. Cao X, Chen W, Zhao P, Yang Y, Yu D-G. Electrospun Porous Nanofibers: Pore−Forming Mechanisms and Applications for Photocatalytic Degradation of Organic Pollutants in Wastewater. Polymers. 2022;14(19):3990. DOI: 10.3390/polym14193990
81. Wang Z, Zhao C, Pan Z. Porous bead-on-string poly(lactic acid) fibrous membranes for air filtration. Journal of Colloid and Interface Science. 2015;441:121-9. DOI: 10.1016/j.jcis.2014.11.041
82. Chen W, Zhao P, Yang Y, Yu D-G. Electrospun beads-on-the-string nanoproducts: Preparation and drug delivery application. Curr Drug Deliv. 2022;19. DOI: 10.2174/1567201819666220525095844
83. Li T, Ding X, Sui X, Tian L, Zhang Y, Hu J, et al. Sustained release of protein particle encapsulated in bead-on-string electrospun nanofibers. J Macromol Sci, Part B: Phys. 2015;54(8):887-96. DOI: 10.1080/00222348.2015.1051210
84. Li T, Ding X, Tian L, Hu J, Yang X, Ramakrishna S. The control of beads diameter of bead-on-string electrospun nanofibers and the corresponding release behaviors of embedded drugs. Materials Science and Engineering: C. 2017;74:471-7. DOI: 10.1016/j.msec.2016.12.050
85. Li T, Ding X, Tian L, Ramakrishna S. Engineering BSA-dextran particles encapsulated bead-on-string nanofiber scaffold for tissue engineering applications. J Mater Sci. 2017;52:10661-72. DOI: 10.1007/s10853-017-1245-9
86. Gunaratne LMWK, Shanks RA. Multiple melting behaviour of poly(3-hydroxybutyrate-co-hydroxyvalerate) using step-scan DSC. Eur Polym J. 2005;41(12):2980-8. DOI: 10.1016/j.eurpolymj.2005.06.015
87. Ding C, Cheng B, Wu Q. DSC analysis of isothermally melt-crystallized bacterial poly (3-hydroxybutyrate-co-3-hydroxyhexanoate) films. J Therm Anal Calorim. 2011;103(3):1001-6. DOI: 10.1007/s10973-010-1135-8
88. Vanheusden C, Samyn P, Goderis B, Hamid M, Reddy N, Ethirajan A, et al. Extrusion and Injection Molding of Poly(3-Hydroxybutyrate-co-3-Hydroxyhexanoate) (PHBHHx): Influence of Processing Conditions on Mechanical Properties and Microstructure. Polymers. 2021;13(22):4012. DOI: 10.3390/polym13224012
89. Minsart M, Van Vlierberghe S, Dubruel P, Mignon A. Commercial wound dressings for the treatment of exuding wounds: an in-depth physico-chemical comparative study. Burns & Trauma. 2022;10. DOI: 10.1093/burnst/tkac024

90. Palangetić L, Clasen C. Electrospinning of polymer solutions: jet stability and novel applications. Leuven: KU Leuven. Faculteit ingenieurswetenschappen; 2014. ISBN: 978-94-6018-903-6